12 June 2009 | $10

Science

AAAS

Leading-Edge Vortices Elevate Lift of Autorotating Plant Seeds

D. Lentink,[1]* W. B. Dickson,[2] J. L. van Leeuwen,[1] M. H. Dickinson[2]

As they descend, the autorotating seeds of maples and some other trees generate unexpectedly high lift, but how they attain this elevated performance is unknown. To elucidate the mechanisms responsible, we measured the three-dimensional flow around dynamically scaled models of maple and hornbeam seeds. Our results indicate that these seeds attain high lift by generating a stable leading-edge vortex (LEV) as they descend. The compact LEV, which we verified on real specimens, allows maple seeds to remain in the air more effectively than do a variety of nonautorotating seeds. LEVs also explain the high lift generated by hovering insects, bats, and possibly birds, suggesting that the use of LEVs represents a convergent aerodynamic solution in the evolution of flight performance in both animals and plants.

Maples (*Acer*) are primary succession trees adapted to nutrient-poor habitats in temperate climates (*1*). Like many other pioneer trees, maples rely on wind, updrafts, and turbulent gusts to disperse their seeds over distances ranging from several meters to kilometers (*2*, *3*). Maple seeds typically disperse under windy conditions and start to autorotate within 1 m of detaching from the tree (Fig. 1, A and C). They autorotate because the heavy nut, and hence the center of gravity, is located at the base of the wing-shaped seed (*4*–*8*). The stable autorotation of maple and other rotary seeds depends on an interplay between their three-dimensional (3D) inertial and aerodynamic properties, which is not fully understood (*4*, *9*, *10*). The presumed function of autorotation is that it creates lift to prolong the descent of the seed. Detailed performance studies (*4*, *6*, *8*) revealed that autorotating seeds are able to generate unexpectedly high lift forces despite their small size and slow velocity. Like autorotating seeds, insect wings generate very high lift despite operating at angles of attack well above those that will stall conventional aircraft wings and helicopter blades (*11*) (Fig. 1D). Instead of stalling, insect wings generate a prominent leading-edge vortex (LEV), which is known to be responsible for elevating both lift and drag (*11*, *12*–*16*). Building upon these observations, we hypothesized that autorotating seeds create a LEV that enables them to generate high lift at high angles of attack during their descent.

To test if autorotating seeds generate a LEV, we built a dynamically scaled model actuated by a robotic arm in a tank of mineral oil (*17*, *18*) (fig. S1). We based the shape of the model on the planform of one individual seed ($n = 1$) and the kinematics on the average free-flight motion of 20 individuals ($n = 20$) from three species of maple (*m1: Acer diabolicum* Blume; *m2: Acer palmatum* Thunb. var. *matsumurae* Makino, and *m3: Acer palmatum* Thunb) and one species of hornbeam (*h*: *Carpinus ischonoskii* Maxim) (Fig. 1B). The seeds from all four of these species are known to generate high lift (*6*, *19*). The flight parameters and the ratio of inertial to viscous stress in the surrounding flow of the model seeds in oil were scaled such that they are identical to real seeds descending in air. This stress ratio is measured by the Reynolds number and is on the order of 1000 for autorotating seeds (*6*). We used stereo digital particle image velocimetry (DPIV) to measure the 3D velocity field at 26 equally spaced spanwise slices starting at roughly 25% span (indicated in green in Fig. 1B) and extending well beyond the wing tip so that we captured the structure of the tip vortex as well. We combined all slices to reconstruct the 3D velocity field around the model seeds (*18*, *20*) (Fig. 2).

Our measurements show that all four model seeds generate a prominent LEV near the base, which is markedly similar to the LEVs produced by insect wings. The structure of the LEV depends not only on the wing shape and Reynolds number, but also on the wing's angle of attack. Because the wing's rotation induces a radial velocity distribution as the seed descends, the angle of attack is maximal at the wing root (~90°) and minimal at the wing tip (Fig. 1D). Based on prior free-flight measurements (*6*, *19*), we calculated the angle of attack at the wing tip to be lowest for maple seed *m1* (16°), highest for hornbeam *h* (28°), and intermediate for the two other maples seeds, *m2* (25°) and *m3* (26°) (*18*). This qualitative trend can explain in part why the LEV of all three maple seeds (Fig. 2, A to C) is relatively compact and well attached to the seed's surface, whereas the LEV generated by the hornbeam seed appears more separated (Fig. 2D). The LEV is most prominent near the base of the seed, shown at 25% span, where there is a strong concentration of vorticity (first row in Fig. 3, A to D). Toward the tip (at 75% span), the LEV merges with the tip vortex, resulting in a long trail of vorticity in the seed's wake. The chordwise flow around the maple seeds reattaches behind the LEV near the trailing edge, whereas the flow around the hornbeam seed is more separated at the wing tip and fails to reattach. This difference in flow structure is also apparent in images of the 3D and 2D streamlines (Fig. 2 and last row in Fig. 3, A to D) and the vorticity plots (first row in Fig. 3, A to D).

To verify that real autorotating seeds do indeed generate a stable LEV during their descent,

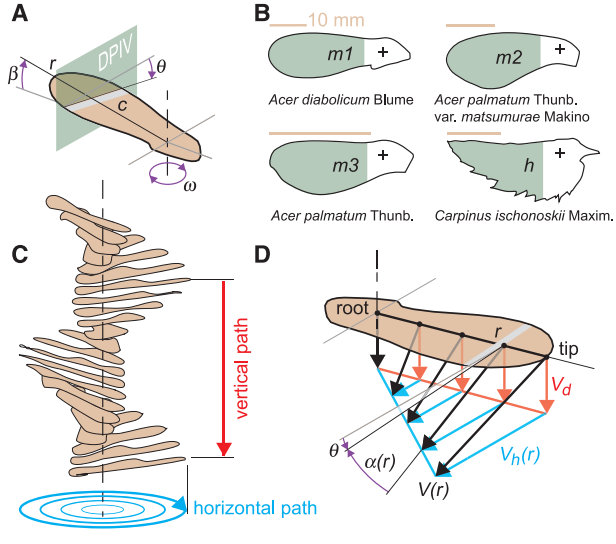

Fig. 1. Kinematics and morphology of all four autorotating seeds studied. (**A**) Free-flight parameters of autorotating seeds [after (*6*)]: local wing radius, *r*; local chord length, *c*; pitch angle, θ; cone angle, β; angular velocity, ω. One of up to 26 planes in which we measured the velocity field along the span using DPIV is indicated in green. (**B**) Planform of the three maple seeds (*m1*, *m2*, *m3*) and hornbeam seed (*h*) studied; the green area indicates the region for which we performed DPIV around the wing. The plus sign indicates the center of gravity, which corresponds closely to the center of rotation (*6*, *8*, *19*). (**C**) Free-flight sequence of an autorotating seed showing both the vertical (red) and horizontal, circular translation (blue) of a wing section during a full period. (**D**) Because of the different horizontal path lengths traveled by subsequent spanwise wing sections (C), the wing's local geometric angle of attack is defined as the arctangent of descent speed, V_d, divided by horizontal speed, V_h. The effective aerodynamic angle of attack, α, is equal to geometric angle of attack minus the absolute value of the pitch angle (*m1*, –1.17°; *m2*, –1.39°; *m3*, –0.90°; *h*, –2.16°), measured at 75% span and approximately constant along span (*6*); α is lowest at the tip and increases toward the base where it approaches 90°. [*V* is velocity and "(*r*)" indicates dependence of a variable on radius.]

[1]Experimental Zoology Group, Wageningen University, 6709 PG Wageningen, Netherlands. [2]Bioengineering and Biology, California Institute of Technology, Pasadena, CA 91125, USA.

*To whom correspondence should be addressed. E-mail: david.lentink@wur.nl

Downloaded from www.sciencemag.org on June 11, 2009

as our model experiments suggest, we built a vertical wind tunnel to study freely flying maple seeds (*Acer pseudo-platanus L.*: *m4*). By matching tunnel speed with the descent rate of the seed, we were able to film 34 seeds spinning at a stationary height in lab frame coordinates (fig. S3) (*18*). The seeds flew at wing-tip angles of attack ranging from 12° to 32° (Reynolds numbers ~ 1000); for 32 of these seeds we successfully visualized the flow around the wing (Fig. 3E; see also movie S1 and fig. S4 for all 32 LEV visualizations) (*18*). These free-flight experiments confirm the findings from our dynamically scaled model that (i) autorotating seeds generate a prominent stable LEV near their base and (ii) the LEV is more compact at lower angles of attack.

How well does the flow structure around the seeds compare to that of insect wings? The gross flow structure shows a prominent LEV (Fig. 2, A and B), as found for insects. For insect wings operating at Reynolds numbers on the order of 100 to 1000, stable attachment of the LEV is thought to depend partly on strong spanwise flow on top of the wing that drains vorticity from the LEV toward the wing-tip vortex (*14*, *21*, *22*). This process, which stretches and tightens the LEV, is a key feature, because it prevents the LEV from growing so large that it becomes unstable and separates. For all four seeds, we found strong spanwise flow on top of the wing (second row in Fig. 3, A to D). The spanwise flow is concentrated in the LEV at 25% span, whereas it is smeared out toward the trailing edge at 50% span and convected into the wake and tip vortex at 75% span—a pattern quite similar to that described for revolving insect wings (*22*).

To find out to which degree the LEV locally amplifies lift over the wing, we computed the seed's spanwise lift distribution by integrating vorticity within each wing section (*18*) (Fig. 4A). Sectional lift displays a clear maximum near 40 to 60% span for maple seeds *m1* and *m2*, whereas it forms a wider plateau for maple seed *m3* and hornbeam seed *h*. The lift distribution for maple seeds *m1* and *m2* resembles that measured on a revolving model fly wing at Reynolds number 1400, which also generates a stable LEV (*22*). The lift distribution is equal to the product of the local chord length, the sectional dynamic pressure, and sectional lift coefficient (*18*) (Fig. 4, B and C). The variation in spanwise lift is less than might be expected, because whereas sectional dynamic pressure rises toward the tip (where local velocities are highest), the sectional lift coefficient rises toward the base (Fig. 4, B and C). This spanwise distribution in lift coefficient is explained largely by the variation in angle of attack, which rises toward the base (Fig. 4D). The sectional lift coefficient reaches very high values ranging from 2 for hornbeam to almost 5 for maple seeds. The flow visualization in Figs. 2 and 3 indicates that the LEV is attached at the 25% span location where the sectional lift coefficient is greatest. The stable attachment of the LEV is noteworthy, given that the local angles of attack are well beyond the stall point for conventional aircraft wings and helicopter blades.

How effectively do these autorotating seeds descend, and how do they perform compared to other autorotating and gliding seeds? For successful dispersion, seeds need to have a long descent time so that the wind can carry them away from their tree of origin. Using a basic aerodynamic performance analysis, Eqs. S1 to S7 (*18*), we show that descent time is inversely proportional to the square root of wing loading (weight per unit surface area) and directly proportional to the square root of the descent factor, a dimensionless number that represents the seed's aerodynamic efficacy for a given descent speed and wing loading. To determine how well autorotating seeds perform, we compared their descent time as a function of wing loading with that of gliding and straying seeds in Fig. 5A. The color-coded hyperbolic lines in Fig. 5 indicate values of constant descent factor and thus constant aerodynamic efficacy. Gliding and straying seeds achieve long descent times, but they do so using low descent factors and thus must operate with very small wing loading, typically much less than 1 N m^{-2}. Because they operate with higher descent factors, autorotating seeds can achieve comparably long descent times at much greater wing loading. For example, the average descent time of autorotating seeds (yellow circle, Fig. 5A) is 36% longer than the value predicted from the low descent factors used by gliding and straying seeds (blue star, Fig. 5A).

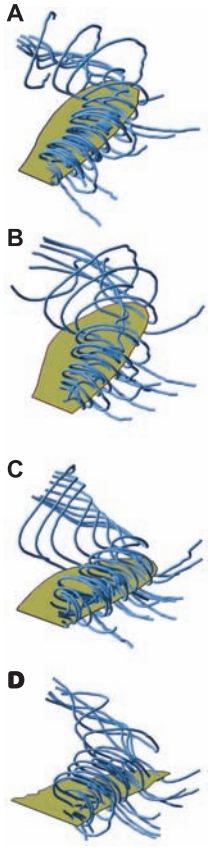

Fig. 2. The large LEV measured for all four model seeds. (**A** to **D**) Flow visualization of absolute (in lab frame) streamlines (shown in blue), calculated from the 3D velocity field measured using DPIV. The models of the three maple seeds [(A) *m1*, (B) *m2*, (C) *m3*] and the hornbeam seed [(D) *h*] generate a LEV with substantial spanwise flow that is connected to the tip vortex. The angle of attack of the seed increases from (A) to (D). Note that the seed spins clockwise (in all figures).

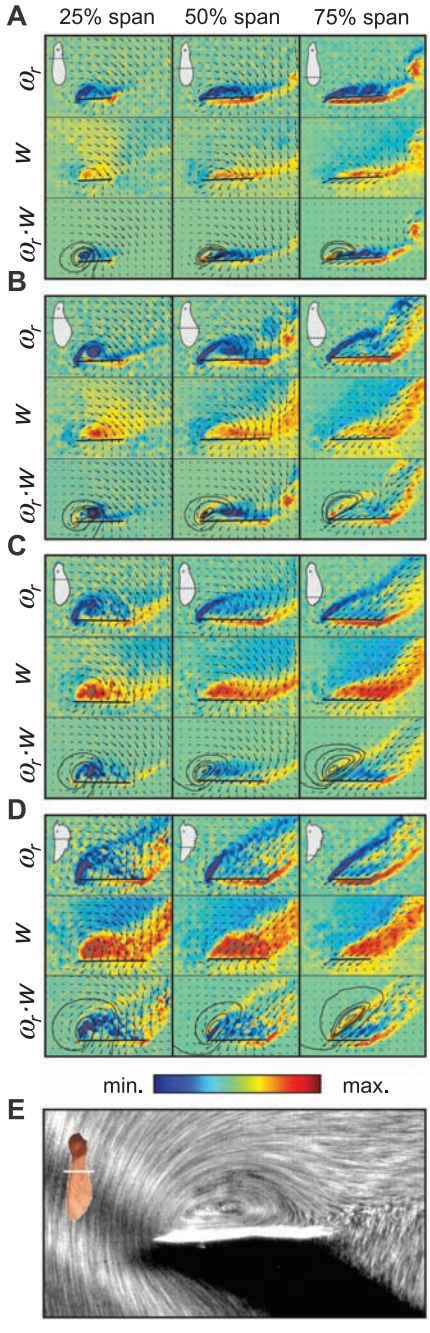

Fig. 3. The vorticity concentration that builds up the LEV at the wing's base is drained by concentrated spanwise flow. (**A** to **D**) Measured flow fields of seeds *m1* (A), *m2* (B), *m3* (C), and *h* (D) subsequently shown in the three columns of every block for three spanwise sections: 25, 50, and 75% span. First row shows spanwise vorticity (ω_r), which builds up into a prominent LEV at 25% span for all four seeds [color bar (A to D): ±70, ±50, ±30, ±30 s^{-1}]. Second row shows spanwise flow speed (w), which peaks at 25% span [color bar (A to D): ±0.5, ±0.4, ±0.2, ±0.2 ms^{-1}]. Third row shows spanwise transport of vorticity ($\omega_r \cdot w$), which peaks at 25% span [color bar (A to D): ±13, ±8, ±3, ±3 ms^{-2}]. (**E**) We found that freely flying *m4* maple seeds in our vertical wind tunnel generated a prominent LEV near the base (n = 32). The angle of attack at the wing tip of this specimen is 20° (between *m1* and *m2*).

Downloaded from www.sciencemag.org on June 11, 2009

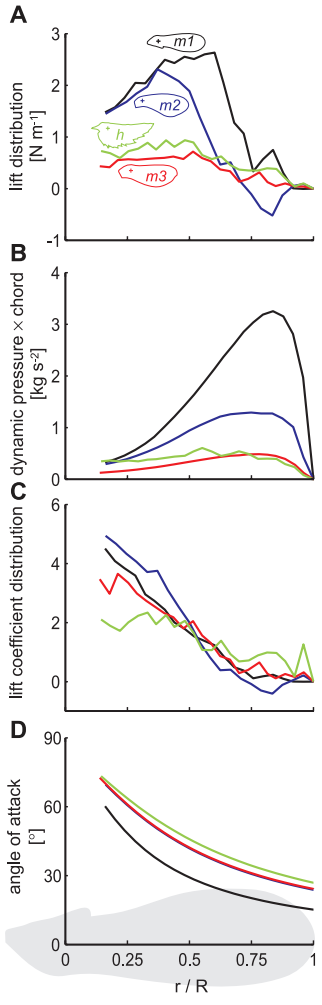

Fig. 4. The LEV induces exceptional high local lift coefficients near the wing's base. (**A**) Spanwise lift distribution. The wing's sectional lift is particularly low near the wing tip due to the presence of the tip vortex (*r*, local radius; *R*, wing-tip radius; seed code, Fig. 1B). (**B**) Product of sectional dynamic pressure and chord length. (**C**) The wing's sectional lift coefficient [(A) divided by (B)] peaks near the wing's base (where a LEV is present) and is minimal at the tip. (**D**) The distribution of angle of attack with span. The high lift coefficients near the base of the wing (C) and the corresponding LEV result from the extremely high local angles of attack, well beyond 30°.

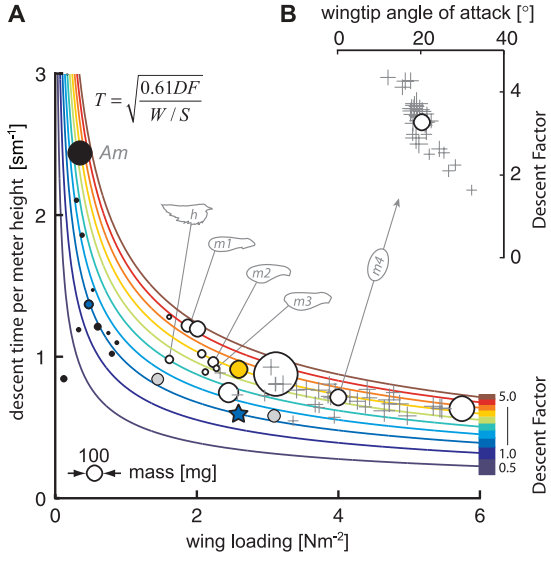

Fig. 5. Autorotating seeds operate at high aerodynamic efficacy, which is greatest at low wing-tip angle of attack. (**A**) Descent time of autorotating seeds (○,+) compared to gliding and straying seeds (●) as a function of wing loading. Symbol width indicates seed mass. Inset equation (see Supporting Online Material) indicates that descent time (*T*) is proportional to the square root of descent factor (*DF*), which is a measure of aerodynamic efficacy, divided by wing loading (*W*/*S*). The average descent time and wing loading of gliding and straying seeds is indicated by the blue circle. The average descent time and wing loading of the autorotating seeds is indicated by the yellow circle. The blue star indicates the predicted performance of gliding and straying seeds if they operated at the wing loading of autorotating seeds. The color-coded hyperbolic curves represent descent time as a function of wing loading at constant descent factor. The flight data have been measured by Azuma and co-workers (*6*, *8*, *29*, *30*), whereas crosses and the corresponding circle of *m4* indicate our vertical wind tunnel measurements of *Acer pseudo-platanus L*. seeds. The spread of the *m4* data illustrates the variance in performance that is typical of seeds (*6*, *8*, *29*, *30*). The specialized gliding seed *Alsomitra macrocarpa* (*Am*) is the only seed in this comparison that does not rely on substantial wind for dispersal (*29*). Ash and tulip tree seeds (gray circles) also autorotate, but spin along two major axes. (**B**) Within a population of *m4* seeds, descent factor increases with decreasing wing-tip angle of attack.

The 100% higher aerodynamic efficacy (on average) of autorotating seeds explains how they can descend only 30% faster than gliding and straying seeds even though their wing loading is 450% higher. Descent factor is highest for maple *m1* and is sequentially lower for *m2*, *m3*, and hornbeam *h*, which operate at higher angle of attacks. The compact and well-attached LEV generated by the maple seeds corresponds to higher aerodynamic efficacy than that of the partially stalled hornbeam seed, neglecting Reynolds number and morphological effects. Our free-flight experiments with 34 *m4* specimens in a vertical wind tunnel confirm this trend: A seed's aerodynamic efficacy increases with decreasing angle of attack (Fig. 5B), because at lower angles the LEV is more compact (fig. S4) (*18*).

The high lift generated by LEVs is exploited not only by autorotating seeds during their descent; hovering insects (*11*, *12*–*16*), bats (*23*), and probably birds (*24*–*27*) use the same mechanism. This suggests that the use of LEVs represents a convergent aerodynamic solution in the evolution of high-performance flight of both animal wings and plant seeds. Our results show that the LEV enhances the descent time of autorotating seeds for a given value of wing loading. This allows a plant to achieve high dispersal performance while investing more resources in each seed's embryo relative to those invested in building the seed's aerodynamic surface. Reliance on a LEV therefore expands the seed dispersal range and most likely the fitness of the tree. The enhanced aerodynamic performance of autorotating seeds could inspire the design of more effective autorotating vehicles (*9*, *28*).

References and Notes

1. L. Van der Pijl, *Principles of Dispersal in Higher Plants* (Springer-Verlag, Berlin, ed. 3, 1982).
2. R. Nathan *et al.*, *Nature* **418**, 409 (2002).
3. R. Nathan, *Science* **313**, 786 (2006).
4. R. A. Norberg, *Biol. Rev. Camb. Philos. Soc.* **48**, 561 (1973).
5. F. M. Burrows, in *Seed Dispersal*, D. R. Murray, Ed. (Academic Press, San Diego, 1986), pp. 1–49.
6. A. Azuma, K. Yasuda, *J. Theor. Biol.* **138**, 23 (1989).
7. K. J. Niklas, *Plant Biomechanics* (Univ. of Chicago Press, Chicago, 1992).
8. A. Azuma, *The Biokinetics of Flying and Swimming* (AIAA Education Series, Reston, VA, ed. 2, 2006).
9. H. J. Lugt, *Annu. Rev. Fluid Mech.* **15**, 123 (1983).
10. D. Seter, A. Rosen, *Trans. ASME* **59**, 1000 (1992).
11. J. R. Usherwood, C. P. Ellington, *J. Exp. Biol.* **205**, 1547 (2002).
12. T. Maxworthy, *J. Fluid Mech.* **93**, 47 (1979).
13. M. H. Dickinson, K. G. Götz, *J. Exp. Biol.* **174**, 45 (1993).
14. C. P. Ellington, C. van den Berg, A. P. Willmott, A. L. R. Thomas, *Nature* **384**, 626 (1996).
15. M. H. Dickinson, F.-O. Lehmann, S. P. Sane, *Science* **284**, 1954 (1999).
16. R. B. Srygley, A. L. R. Thomas, *Nature* **420**, 660 (2002).
17. W. B. Dickson, M. H. Dickinson, *J. Exp. Biol.* **207**, 4269 (2004).
18. Materials and methods are available as supporting material on *Science* Online.
19. K. Yasuda, A. Azuma, *J. Theor. Biol.* **185**, 313 (1997).
20. C. Poelma, W. B. Dickson, M. H. Dickinson, *Exp. Fluids* **41**, 213 (2006).
21. J. M. Birch, M. H. Dickinson, *Nature* **412**, 729 (2001).
22. J. M. Birch, W. B. Dickson, M. H. Dickinson, *J. Exp. Biol.* **207**, 1063 (2004).
23. F. T. Muijres *et al.*, *Science* **319**, 1250 (2008).
24. J. J. Videler, E. J. Stamhuis, G. D. E. Povel, *Science* **306**, 1960 (2004).
25. D. R. Warrick, B. W. Tobalske, D. R. Powers, *Nature* **435**, 1094 (2005).
26. T. Hubel, thesis, TU Darmstadt, Fachbereich Biologie, Germany (2006).
27. D. Lentink *et al.*, *Nature* **446**, 1082 (2007).
28. R. D. Lorenz, *Spinning Flight* (Springer, New York, 2006).
29. A. Azuma, Y. Okuno, *J. Theor. Biol.* **129**, 263 (1987).
30. S. Minami, A. Azuma, *J. Theor. Biol.* **225**, 1 (2003).

31. We thank M. Lino, E. W. Karruppannan, E. Janssen, J. G. M. van den Boogaart, K. M. Leon, and H. Schipper for help with the free-flight experiments. We thank G. E. Elsinga, J. R. Usherwood, and G. J. F. van Heijst for valuable comments. Research was funded by Netherlands Organisation for Scientific Research–Earth and Life Sciences Council (NWO-ALW, grant 817.02.012) (to D.L. and J.L.v.L.) and NSF grant IBN-0217229 (to M.H.D.).

Supporting Online Material

www.sciencemag.org/cgi/content/full/324/5933/1438/DC1
Materials and Methods
Figs. S1 to S7
Equations S1 to S7
References

30 March 2009; accepted 14 May 2009
10.1126/science.1174196

Downloaded from www.sciencemag.org on June 11, 2009

EXTENDED PDF FORMAT
SPONSORED BY
usb
www.usbweb.com

Leading-Edge Vortices Elevate Lift of Autorotating Plant Seeds

D. Lentink, *et al.*

Science **324**, 1438 (2009);
DOI: 10.1126/science.1174196

The following resources related to this article are available online at www.sciencemag.org (this information is current as of June 11, 2009):

Updated information and services, including high-resolution figures, can be found in the online version of this article at:
http://www.sciencemag.org/cgi/content/full/324/5933/1438

Supporting Online Material can be found at:
http://www.sciencemag.org/cgi/content/full/324/5933/1438/DC1

This article **cites 23 articles**, 8 of which can be accessed for free:
http://www.sciencemag.org/cgi/content/full/324/5933/1438#otherarticles

This article appears in the following **subject collections**:
Botany
http://www.sciencemag.org/cgi/collection/botany

Information about obtaining **reprints** of this article or about obtaining **permission to reproduce this article** in whole or in part can be found at:
http://www.sciencemag.org/about/permissions.dtl

Downloaded from www.sciencemag.org on June 11, 2009

Science (print ISSN 0036-8075; online ISSN 1095-9203) is published weekly, except the last week in December, by the American Association for the Advancement of Science, 1200 New York Avenue NW, Washington, DC 20005. Copyright 2009 by the American Association for the Advancement of Science; all rights reserved. The title *Science* is a registered trademark of AAAS.